Modifying the electronic structure of TiS$_2$ by alkali metal intercalation

Modifying the electronic structure of TiS$_2$ by alkali metal intercalation

H E Brauer†, H I Starnberg†¶, L J Holleboom‡, H P Hughes§ and
V N Strocov‖

† Department of Physics, Göteborg University and Chalmers University of Technology,
SE-412 96 Göteborg, Sweden
‡ Department of Theoretical Physics, University of Lund, SE-223 62 Lund, Sweden
§ Cavendish Laboratory, University of Cambridge, Madingley Road, Cambridge CB3 0HE, UK
‖ Institute for High-Performance Computations and Data Bases, PO Box 76,
194291 St Petersburg, Russia

Abstract.   Angle-resolved photoelectron spectroscopy has been used to study *in situ* intercalation of the layered compound TiS$_2$ with Na and Cs. The intercalation was verified by core-level spectroscopy. The valence bands of pure TiS$_2$ and the intercalated compounds Na$_x$TiS$_2$ and Cs$_x$TiS$_2$ were characterized and compared to self-consistent LAPW band-structure calculations. Remarkable agreement between experimental and calculated bands was found for the dispersion along the layers. The calculations predicted perpendicular dispersion also for the intercalation compounds, although significantly reduced. No significant perpendicular dispersion was seen in normal-emission spectra, which might be an effect of intercalation-induced stacking disorder. Charge transfer to the TiS$_2$ host layers was evident from the much increased conduction band emission, and from the asymmetric S 2p core-level lineshape after intercalation. The intercalation produced electronic structure changes which are not well described by the rigid-band model, but as these changes occur at an early stage, the model can still be used, with modified bands, to describe the continued intercalation.

1. Introduction

TiS$_2$ is one of the most studied layered transition metal dichalcogenides (TMDCs), experimentally as well as theoretically. Earlier, there was controversy over whether TiS$_2$ is a semimetal or a semiconductor, but the existence of an indirect band gap ($\sim$0.2 eV) has since then been established by angle-resolved photoelectron spectroscopy (ARPES) and measurements of transport properties [1–3]. In practice there is always some excess Ti present, leading to partial filling of the Ti 3d conduction band and degenerate extrinsic behaviour. TiS$_2$ crystallizes in the 1T-CdI$_2$ structure, shown in figure 1, with each layer consisting of a hexagonal Ti sheet sandwiched between two S sheets, positioned so as to make each Ti atom octahedrally coordinated by six S atoms. Bonding is strong within each layer, but adjacent layers are held together by weak van der Waals-like interactions only.

The TMDCs exhibit a rich variety of interesting phenomena, e.g. superconductivity, periodic lattice distortions and charge-density waves. Particularly interesting is the possibility of forming intercalation complexes [4–7], in which foreign atoms or molecules enter the

¶ Author to whom any correspondence should be addressed.

1T-TiS$_2$ 1T-ATiS$_2$
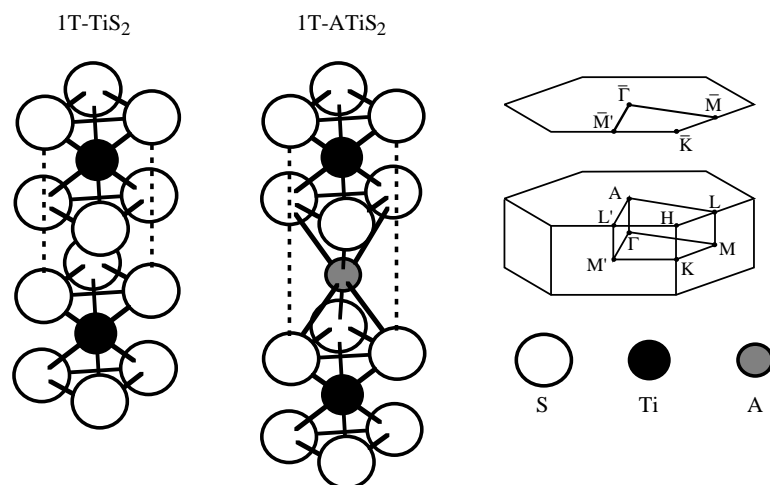
Figure 1. The crystallographic structure of 1T-TiS$_2$ and the assumed 1T structure of alkali-metal-intercalated TiS$_2$. 'A' = Na or Cs. The corresponding surface and bulk Brillouin zones are shown in the upper right corner.

interlayer gaps. Much work has been done on TMDCs intercalated by electrochemical or related methods, but these methods have usually not provided high-quality single-crystal samples suitable for investigation by surface science techniques. This limitation has recently been overcome by the *in situ* intercalation technique, which involves ultrahigh-vacuum (UHV) deposition of alkali or noble metals onto TMDC surfaces, followed by spontaneous intercalation [8–11]. In particular, the application of ARPES to TMDCs intercalated *in situ* has provided very detailed knowledge about the electronic structure of several TMDC intercalation systems [12–17]. We here report ARPES results for TiS$_2$ before and after *in situ* intercalation with Na and Cs, together with self-consistent band-structure calculations for TiS$_2$, NaTiS$_2$ and CsTiS$_2$. One motive for this study is that the electronic structure information obtained about TiS$_2$ intercalation systems should be useful for systematic comparison with other similar systems. The properties of TiS$_2$ and its intercalation compounds are also of particular interest, as TiS$_2$ is often seen as a prototype of the TMDCs, and as it is one of the most interesting TMDCs for practical applications.

2. Band-structure calculations

2.1. Method and crystal structures

Self-consistent scalar-relativistic [18] band structures of TiS$_2$ and the hypothetical compounds NaTiS$_2$ and CsTiS$_2$ were calculated by the linear augmented-plane-wave (LAPW) method, within the local density approximation (LDA) of density functional theory. Spin–orbit splitting was not included. The calculations used 65 k-points in the irreducible part of the Brillouin zone (BZ) together with 400 LAPW basis functions. The parametrized Ceperley–Alder form [19] of the exchange–correlation potential was used. The calculations were of full-potential type, i.e. not restricted to muffin-tin-type potentials, which would have reduced the accuracy for these highly anisotropic materials.

To limit the calculational effort, the 1T layer stacking was retained in the NaTiS$_2$ and CsTiS$_2$ band-structure calculations, despite the fact that 3R stackings have been observed in

TiS$_2$ intercalated with Na and Cs [20, 21]. This simplification is reasonable if the interactions between layers are weak enough that the band structure is not significantly affected by stacking changes. The lattice parameters used for TiS$_2$ were 3.40 Å and 5.70 Å for the *a*- (in-plane) and *c*- (interlayer) axes, respectively [4]. The *a*-axis parameter was increased to 3.46 Å for both NaTiS$_2$ and CsTiS$_2$, while the *c*-axis parameter was increased to 6.43 Å for NaTiS$_2$ and 8.41 Å for CsTiS$_2$. These estimates were based upon comparisons with other alkali metal intercalates [6, 7, 22] and ionic radii considerations [23]. The 1T structures are illustrated in figure 1, together with the corresponding surface and bulk BZs.

A common problem of LDA band-structure calculations is their tendency to underestimate semiconductor band gaps. When comparing with experimental data, this can be compensated for by shifting the conduction bands rigidly relative to the valence bands until the best possible agreement is achieved (as is done in section 5).

2.2. TiS$_2$

Figure 2(a) shows our calculated LAPW bands for TiS$_2$. At (and above) the Fermi energy E_F, five Ti 3d-derived conduction bands are found, and immediately below there are six valence
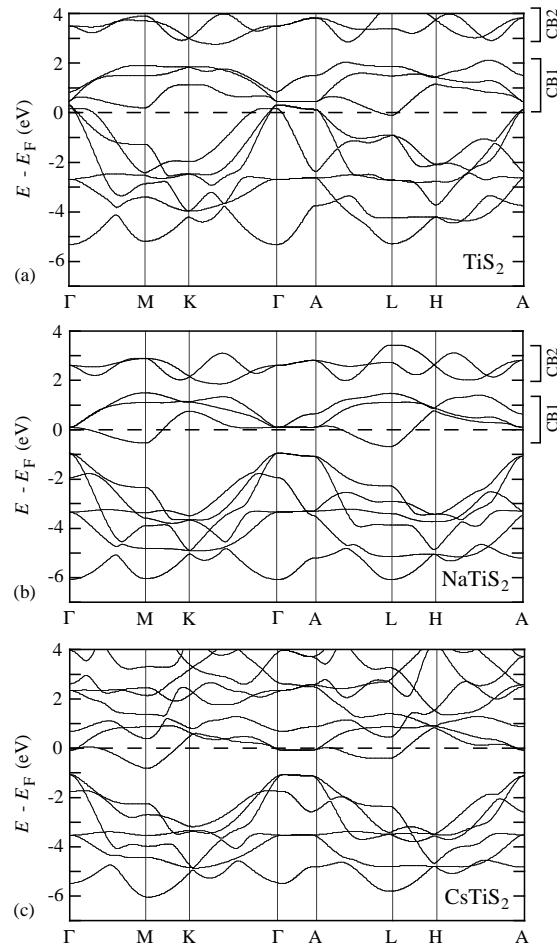
Figure 2. Calculated band structures of (a) TiS$_2$, (b) NaTiS$_2$ and (c) CsTiS$_2$.

bands of predominantly S 3p character. The latter are strongly dispersive throughout the BZ, two of them also along ΓA (perpendicular to the layers). The conduction bands can be divided into two groups, CB1 with three bands in the range 0–2 eV and CB2 with two bands 3–4 eV above E_F. Above the CB2 bands is a 1.5 eV fundamental gap. Due to the LDA band-gap problem, the calculated valence and conduction bands overlap, despite the experimentally verified indirect band gap. In addition to the bands shown, the calculation also produced two S 3s-derived bands 11.5–13.5 eV below E_F. Our calculated bands are similar to those of several other calculations [24–32], which differ mainly as regards the size of the band gap (or overlap).

2.3. NaTiS$_2$ and CsTiS$_2$

The LAPW bands of NaTiS$_2$ and CsTiS$_2$ are shown in figures 2(b) and 2(c). Several significant changes as compared to TiS$_2$ can be seen. The separation between valence and conduction bands is increased by $\sim$0.6 eV, thereby removing the overlap, and the total valence bandwidth is reduced by $\sim$0.5 eV for both compounds. The lowest conduction bands becomes half-filled, which should result in metallic behaviour. Along ΓA the dispersion of those bands which disperse at all is strongly reduced, more so for CsTiS$_2$ than for NaTiS$_2$.

A closer inspection reveals notable differences between the two compounds, despite the general similarity: for NaTiS$_2$ the fundamental gap above CB2 is reduced to $\sim$0.9 eV, while for CsTiS$_2$ it is completely removed by hybridization with bands of Cs 6s, 5d and 4f character. The half-filled lowest conduction band has its minimum at L for NaTiS$_2$ (as for TiS$_2$), while for CsTiS$_2$ the minimum is at M. Along ΓA, the same band is completely above E_F for NaTiS$_2$ but completely below for CsTiS$_2$, rendering the latter compound a more complicated Fermi surface. Although the total valence bandwidths are almost the same, the CsTiS$_2$ valence bands appear somewhat narrower over large parts of the BZ. The S 3s bands (not shown) are less dispersive and in the range 12.6–14.3 eV below E_F for NaTiS$_2$ (12.6–14.4 eV below E_F for CsTiS$_2$), but are otherwise very similar to their TiS$_2$ counterparts. In addition, three bands of Cs 5p character are found 9.2–12.6 eV below E_F for CsTiS$_2$, but given that the large ($\sim$1.5 eV) Cs 5p spin–orbit splitting was neglected, these bands are not expected to be accurate. Some calculated band-structure characteristics of TiS$_2$, NaTiS$_2$ and CsTiS$_2$ are summarized in table 1.

Table 1. Calculated band-structure characteristics of pure and alkali-metal-intercalated TiS$_2$. All entries are binding energies (relative to E_F) in eV. Values for the highest and lowest S 3p bands at each symmetry point are separated by a solidus.

		TiS$_2$	NaTiS$_2$	CsTiS$_2$
Ti 3d	M	−0.2	0.5	0.9
	L	0.1	0.7	0.4
S 3p	Γ	−0.3/5.4	0.9/6.1	1.1/5.5
	A	−0.1/3.8	1.1/5.2	1.1/4.9
S 3p	M	1.3/5.2	2.3/6.1	2.3/6.1
	L	0.9/5.4	2.3/6.1	2.4/5.9
S 3p	K	2.0/4.3	3.5/5.1	3.2/5.0
	H	2.1/4.3	3.4/5.0	3.5/4.8

Our NaTiS$_2$ bands are similar to those calculated by Dijkstra *et al* [31], using the augmented-spherical-wave (ASW) method. Compared to our results, the latter calculation resulted in larger p–d gaps and partial occupation of two bands along ΓA, resulting in significantly different Fermi surfaces.

3. Experimental details

Most of the ARPES experiments were performed at beamline 41 at the MAX synchrotron radiation facility in Lund. The beamline includes a toroidal grating monochromator providing photons with energies in the range 15–200 eV. The synchrotron radiation was polarized in the plane of incidence. Additional measurements were made using unpolarized He I radiation ($h\nu = 21.22$ eV) from a rare-gas discharge lamp. The incidence angle of the light was $\psi = 45°$, unless otherwise stated. The electron energy analysers used had $\pm 2°$ angular acceptance and typically 0.1 eV energy resolution. The spectrometer base pressure was typically 1×10^{-10} Torr.

The TiS$_2$ single crystals were attached to the sample holders with silver-filled epoxy resin. Clean mirrorlike (0001) surfaces were obtained by cleavage *in situ*. The samples were oriented in the $\bar{\Gamma}\bar{K}$ and $\bar{\Gamma}\bar{M}$ (or $\bar{\Gamma}\bar{M}'$) azimuths by LEED which showed a sharp hexagonal 1×1 pattern with low background intensity. The inequivalent $\bar{\Gamma}\bar{M}$ and $\bar{\Gamma}\bar{M}'$ crystallographic directions were identified as described by Law *et al* [33]. The sample used for intercalation with Na was nominally of composition Ti$_{1.008}$S$_2$, while the estimated composition of the ones used with Cs was Ti$_{1.02}$S$_2$. Na and Cs were deposited from carefully outgassed SAES getter sources positioned about 15 mm in front of the sample. The depositions were uncalibrated, but from previous experience each cycle should be equivalent to far more than one-monolayer coverage. The samples were held at room temperature at all times.

The TiS$_2$ surface is known to be chemically very inert, but the alkali-dosed surfaces turned out to be remarkably inert as well. We observed only moderate contamination and no significant surface degrading even 50 h after the initial alkali deposition. This inertness is related to the absence of metallic overlayers at room temperature. The LEED patterns remained sharp but less intense after intercalation. The background intensity increased somewhat, but no superlattice spots were observed.

4. Experimental results

4.1. Core levels

Figure 3(a) shows the Na 2p core level recorded with $h\nu = 82$ eV. Spectrum (i), recorded immediately after an initial Na deposition (2×2 min at 6.0 A) shows a prominent peak (I) at 30.6 eV binding energy (BE), and a broader peak (S) at 32.2 eV BE. In spectrum (ii), recorded ~24 h later, peak S has almost vanished and also peak I appears less intense.

Figure 3(b) shows Cs 4d core-level spectra recorded with $h\nu = 100$ eV (second-order grating diffraction). In spectrum (i), obtained after one Cs deposition (6.0 A for 2 min), four peaks are seen. The Cs 4d level is spin–orbit split by 2.25 eV, and each component is further split into one sharper and one broader peak (with the latter at slightly higher BE). In analogy with the Na 2p case, the Cs 4d$_{5/2}$ peaks are labelled I$_1$ and S$_1$, and the Cs 4d$_{3/2}$ peaks are labelled I$_2$ and S$_2$. In spectrum (ii), recorded after one additional deposition (6.0 A for 4.5 min), peaks I$_1$ and I$_2$ remain at 75.7 and 77.9 eV BE, respectively, while S$_1$ and S$_2$ have increased and shifted so close to the other peaks that these are almost reduced to shoulders.

Figure 3(c) shows the spin–orbit-split S 2p core level recorded with $h\nu = 176$ eV. Spectrum (i) is from pure TiS$_2$, while (ii) was recorded immediately after the initial Na deposition (2×2 min at 6.0 A). The intercalation caused the S 2p level to shift towards lower BE, with the lineshape becoming more asymmetric and a shoulder appearing on the low-BE side. In spectrum (iii), which was measured 24 h later, the shift was reversed and the shoulder reduced, but the asymmetry remained.

Figure 3(d) shows Ti 3p core-level spectra recorded with $h\nu = 110$ eV. Already in
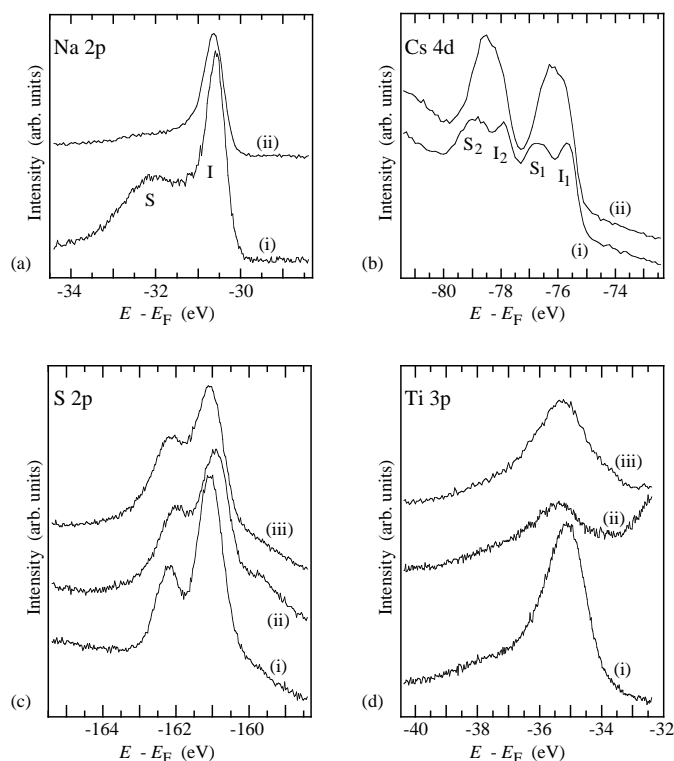
Figure 3. Core level spectra: (a) Na 2p with $h\nu = 82$ eV immediately after Na deposition (i) and ∼24 h later (ii); (b) Cs 4d with $h\nu = 100$ eV (second-order grating diffraction) after one (i) and two (ii) Cs depositions, respectively; (c) S 2p with $h\nu = 176$ eV for pure TiS_2 (i), immediately after Na deposition (ii) and ∼25 h later (iii); (d) Ti 3p with $h\nu = 110$ eV for pure TiS_2 (i), immediately after Na deposition (ii) and ∼25 h later (iii).

spectrum (i), which was obtained from pure TiS_2, the lineshape was broad and asymmetric. In spectrum (ii) recorded after the initial Na deposition, the Ti 3p signal appears strongly damped and shifted towards higher BE. The intensity increase seen on the low-BE side was caused by the Na 2p level. Spectrum (iii) shows that the Ti 3p signal had recovered 24 h later, but the peak still appears broader and more asymmetric than for the clean TiS_2.

4.2. Valence bands

We have recorded numerous energy distribution curves (EDCs) from pure and intercalated TiS_2 to probe the valence band dispersion. The dispersion perpendicular to the layers (along ΓA) was studied by measuring normal-emission series with varying photon energies, while the parallel dispersion (along $\bar{\Gamma}\bar{K}$, $\bar{\Gamma}\bar{M}$ and $\bar{\Gamma}\bar{M}'$ azimuthal directions) was studied by recording angular series with constant photon energy.

Figure 4(a) shows normal-emission EDCs for pure TiS_2. Two strongly dispersive peaks can be seen at about 2 and 5 eV BE. Two conspicuous, but rather dispersionless peaks are seen at ∼1 and ∼3.7 eV BE, respectively, and a weak structure at 0.4 eV BE is also visible. No emission from conduction band states was observed at normal emission.

Figures 4(b) and 4(c) shows analogous normal-emission series of EDCs for TiS_2 intercalated with Na and Cs, respectively. Obviously the perpendicular dispersion is drastically
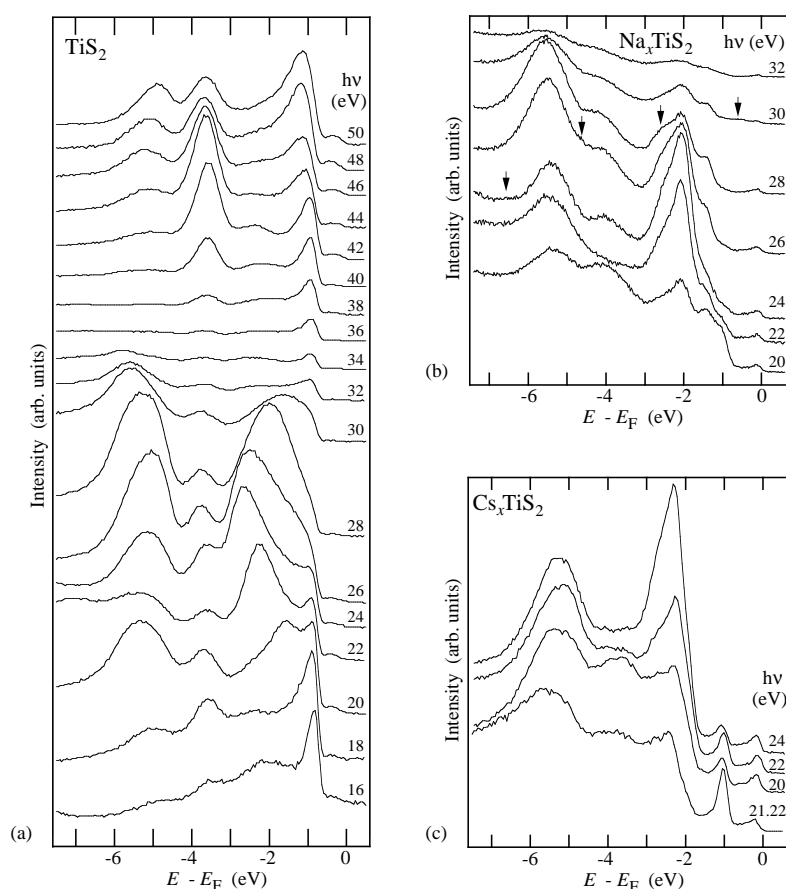
Figure 4. Normal-emission valence band EDCs from: (a) TiS$_2$ with $h\nu = 16$–50 eV; (b) Na$_x$TiS$_2$ with $h\nu = 20$–32 eV (with second-order Na 2p emission indicted by arrows); (c) Cs$_x$TiS$_2$ with $h\nu = 20$–24 eV.

reduced. An overall similarity between Na$_x$TiS$_2$ and Cs$_x$TiS$_2$ is found, but a notable difference is that the feature at $\sim$1 eV BE is very clearly split off from the rest of the valence band in Cs$_x$TiS$_2$, while it is only a weak double structure in Na$_x$TiS$_2$. Conduction band emission just below E_F is seen at all photon energies for both intercalates. Interfering Na 2p emission, excited by second-order grating diffraction, is indicated by arrows in figure 4(b).

Instead of showing our angular series of EDCs explicitly, we have condensed our results into structure plots, as described and discussed in section 5. Some of the raw data have been published elsewhere [15, 34], and our results for pure TiS$_2$ were in good agreement with previous angle-resolved studies [1, 2, 35–37].

5. Discussion

5.1. Probing the intercalation process by core-level spectroscopy

It is well established from earlier alkali/TMDC core-level studies [10, 13, 14, 17, 38, 39] that the core-level peaks of intercalated alkali metals have $\sim$1 eV lower binding energy than the

corresponding peaks of surface-adsorbed alkali species. The intercalation peaks are usually sharper than the surface-related ones, as the intercalated state is more uniform and well defined. In accordance with this, we can identify the peaks labelled I (with subscripts for Cs 4d) in figures 3(a) and 3(b) as due to intercalated alkali metals, while the peaks labelled S are indicative of alkali species on the surface. When comparing the relative intensities of surface and intercalation peaks, one must bear in mind that the latter are significantly reduced by the photoelectrons having to pass through at least one full host layer. It is therefore clear from figure 3(a) that most of the Na intercalated directly after the deposition, and that almost no Na remained on the surface after 24 h. Taking into account both the damping of the intercalation peak and the sloping background in figure 3(b), it is evident that most of the deposited Cs also intercalated rapidly, although the surface-adsorbed fraction was not seen to decrease with time to the same extent as for Na. The shifting of the Cs surface peak towards lower binding energy, which is clearly visible when comparing spectra (i) and (ii) in figure 3(b), indicates that the chemical environment of the adsorbed Cs is changing with time (and the number of depositions). Whether these changes are due to surface contamination or adsorption site alterations (or both) is still not completely settled. However, the corresponding valence band spectra show no significant evidence for surface contamination, despite the fact that in principle they should be highly sensitive to adsorbed contaminants. The explanation in terms of adsorption site changes has gained in credibility from the observation at low temperature of several distinct phases of adsorbed Cs on the TiS_2 surface [39], and from the recent observation of intercalation-induced creation of defects in the Cs/TiS_2 system [40].

It is interesting to compare with the recently reported *in situ* intercalation of VSe_2 with Na, K and Cs [17]. VSe_2 is a metal with the lowest V 3d band half-filled already before intercalation, but the intercalation reaction proceeds in a very similar fashion despite this fundamental difference. The Na 2p and Cs 4d BEs of the intercalated species are identical to within 0.1 eV for both host materials, and the tendency of the surface-related peak to shift towards lower BE with time is observed also for VSe_2. An unexpected finding for VSe_2 was that the intercalation with K appeared to be much slower than with Na or Cs, and also that an exchange reaction took place as Na was deposited on samples already intercalated with K [41]. Preliminary trials suggest that intercalation with K is slower than with Na or Cs also for TiS_2, although the difference between the alkali metals is not quite as pronounced for this host material. It is notable that, although Na was intercalated almost completely in both host materials, the Na remained on the TiS_2 surface for a significantly longer time. This might indicate that the intercalation threshold energy is higher for TiS_2 than for VSe_2.

5.2. S 2p and Ti 3p core levels: screening, energy shifts and broadening mechanisms

Due to the better resolution than in earlier XPS studies [42, 43], the spin–orbit splitting ($\sim$1.2 eV) of the S 2p core level is very clearly seen in figure 3(c). The lineshape in spectrum (i), measured from pure TiS_2, is fairly symmetrical, although a pronounced tail on the low-BE side of spectrum (i) suggests the presence of a component with lower BE than the main peaks. Upon intercalation with Na the main peaks shifted 0.2 eV towards lower BE, and became broader and more asymmetric, as seen in spectrum (ii). The tail on the low-BE side became more prominent as well. Spectrum (iii) in figure 3(c) shows that the asymmetric lineshape remained after 24 h (when almost no Na was left on the surface), but the main peaks were shifted back almost to their positions in spectrum (i), and the low-BE tail lost much of the additional intensity observed in spectrum (ii). In order to quantify the lineshape changes we attempted fitting of the S 2p spectra with Voigt functions. The fitting was done using an exponential background, a fixed spin–orbit splitting of 1.16 eV, the ideal branching ratio 1/2 and a fixed Gaussian width

of 0.70 eV. The singularity index of the peaks was set manually in a trial-and-error fashion. The fitting is illustrated in figure 5. Panel (i) shows the result when two pairs of symmetric peaks were fitted to the experimental spectrum from pure TiS_2. The residual, shown below the fitted curve, is dominated by random noise, which confirms the quality of the fit. Peak A, at 10.34 eV kinetic energy (the peak positions given in this paragraph are for the $2p_{3/2}$ components) and 0.24 eV Lorentzian width, contains ∼90% of the total intensity, while peak B, at 11.35 eV and 0.6 eV Lorentzian width, provides the remaining 10%. Panel (ii) shows the best fit achieved for Na_xTiS_2 (the same spectrum as (iii) in figure 3(c)), using two pairs of peaks. This fit is not satisfactory at all, as the residual shows conspicuous remaining structure, of which part resembles a spin–orbit doublet at higher BE than peak A. An alternative fit to the same spectrum, using three pairs of peaks, was much more successful, as can be seen in panel (iii). To the eye, only random noise is seen in the residual, and the quality measure used by the fitting software (the sum of the squares of the residual divided by the number of points) dropped from 1.21 to 0.31 (the corresponding figure for fit (i) was 0.45, but comparison between different spectra could be misleading). A singularity index of 0.16 was used in both fits to the Na_xTiS_2 spectrum. In summary, fit (iii) produced peak A at 10.42 eV and 0.24 eV Lorentzian width with ∼70% of the intensity, peak B at 11.62 eV and 0.8 eV Lorentzian width
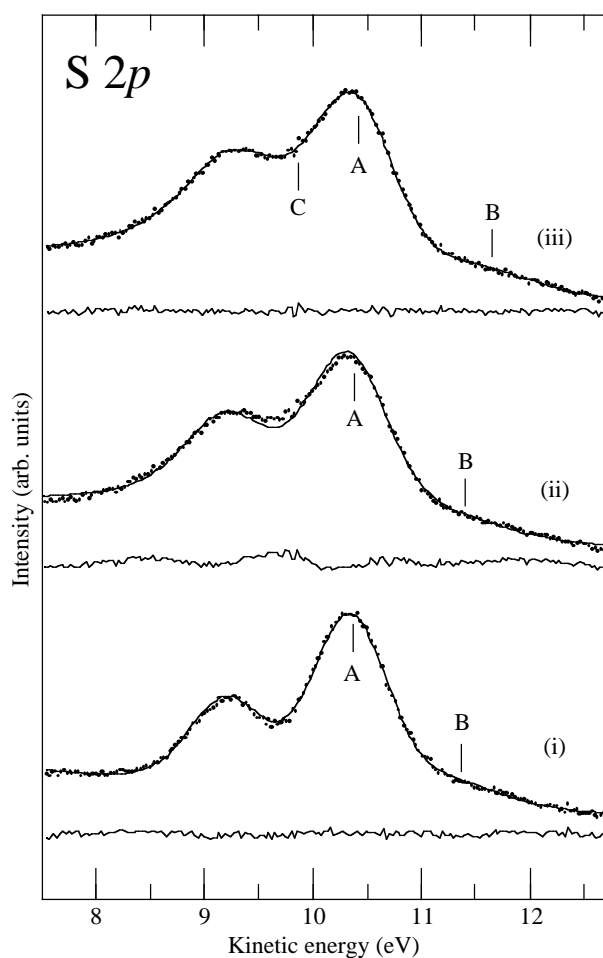
Figure 5. Fitting of experimental S 2p data (dots) with Voigt functions (lines). (i) The spectrum from pure TiS_2, fitted with two pairs of peaks. (ii) The spectrum from Na_xTiS_2, fitted with two pairs of peaks. (iii) The same spectrum as in (ii), but fitted with three pairs of peaks. The residues are shown immediately below the fitted spectra.

with ~20% of the intensity and peak C at 9.87 eV and 0.24 eV Lorentzian width contributing ~10%. The presence of peak B also in the spectrum from pure TiS_2, despite the fact that all surface S sites should be equivalent, suggests that it is produced by defects already present in the outermost layer before intercalation. Regarding peak C in the spectrum from Na_xTiS_2, it should be stressed that caution is advised when interpreting fitted peaks which are not obvious to the eye, but the drastic improvement obtained in the fit quality and the striking indications of high-BE peaks seen in the residual of fit (ii) suggest strongly that this peak is real and not merely an effect of asymmetric broadening. Asymmetric broadening is expected upon intercalation, as the associated population of the lowest Ti 3d band should lead to metallic screening and many-electron excitations within the conduction band [44–46], but the revealed peak-like contribution to the lineshape is not compatible with this mechanism, as the occupied Ti 3d bandwidth is very small. An explanation for the emergence of peak C could be bulk S atoms made inequivalent through different coordination with intercalated Na, or through changes in the layer stacking, as discussed in section 5.3.3. Considering this and the changes with time seen already in figure 3(c), it appears that the main-peak shift and the low-BE structure are mainly associated with Na adsorbed on the surface, while the S 2p asymmetric two-component lineshape is a genuine feature of the intercalation compound. Similar effects of intercalation with Cs have been reported elsewhere [39].

The anomalous weakening of the Ti 3p core level upon alkali metal deposition, which is seen in figure 3(d), can be explained by a very short lifetime of the core hole. Generally, the first-row transition metals have broadened 3p lineshapes due to rapid core-hole decay through super-Coster–Kronig Auger transitions involving 3d states [47]. The Ti 3d-derived conduction band of TiS_2 is nominally empty, but hybridization with the S 3p states mixes some Ti 3d character into the valence band, which enables this broadening mechanism to occur already for pure TiS_2. Upon intercalation, the population of Ti 3d states, and hence the broadening of the Ti 3p spectrum (ii), is drastically increased. Spectrum (iii) shows the recovery of the Ti 3p emission after 24 h, which indicates reduced conduction band filling as the intercalated Na migrates deeper into the sample. Cs intercalation has previously been found to have exactly the same effect [39], and analogous results were also obtained from the $Cs/ZrSe_2$ system [13].

5.3. Modifications of the electronic structure

5.3.1. Agreement with calculations.   For pure TiS_2, several experimental band-structure studies by ARPES [1, 2, 35–37, 48, 49], inverse photoemission [50, 51] and target current spectroscopy [52] have been reported. Of the ARPES studies, only two [36, 37] exploited the possibility, offered by tunable synchrotron radiation, to probe the valence bands perpendicular to the layers. The presence of strongly dispersive peaks in our normal-emission spectra from pure TiS_2, shown in figure 4(a), clearly proves the 3D character of the TiS_2 valence bands. However, the unoccupied bands of the TMDCs are generally too complicated to be well approximated by free-electron parabolas, and consequently the mapping of perpendicular band dispersion becomes problematic. However, it was recently demonstrated that perpendicular bands can be accurately mapped by combining ARPES measurements with very-low-energy electron diffraction (VLEED) [53, 54]. Application of this approach to TiS_2 verified that our LAPW results describe the perpendicular dispersion adequately, although the experimental dispersion of the lowest S 3p band was reduced by large core-hole absorption, and the minimum of the upper dispersive S 3p band was found 0.6 eV higher than the calculated value [55]. The normal-emission spectra of Na_xTiS_2 and Cs_xTiS_2 in figures 4(b) and 4(c) do not show any significant dispersion, which indicates that the intercalation induces a transition from 3D to

2D character of the valence band. This transition, which has been observed previously for several alkali/TMDC systems [12–14, 17], is not fully reflected in the LAPW calculations, which still produce bands with perpendicular dispersion, although significantly reduced. This discrepancy is further discussed in section 5.3.3.

The EDCs in the angular series were reduced into structure plots with the initial energy plotted versus $k_\parallel$. For each peak, $k_\parallel$ (in Å^{-1}) was obtained as $k_\parallel = 0.512\sqrt{E_k} \sin\theta$, with E_k in eV [56]. The TiS$_2$ structure plots in the $\bar{\Gamma}\bar{K}\bar{M}$ and $\bar{\Gamma}\bar{M}$ directions are compared with the LAPW bands in figure 6. As $k_\perp$ is undetermined in the experiments, we compare our experimental points with the LAPW bands in the ΓMK (full lines) and ALH (dashed lines) symmetry planes of the BZ. For constant $k_\parallel$, the minimum and maximum energies of each band are, with few exceptions, in these planes, and the experimental points appearing in the shaded
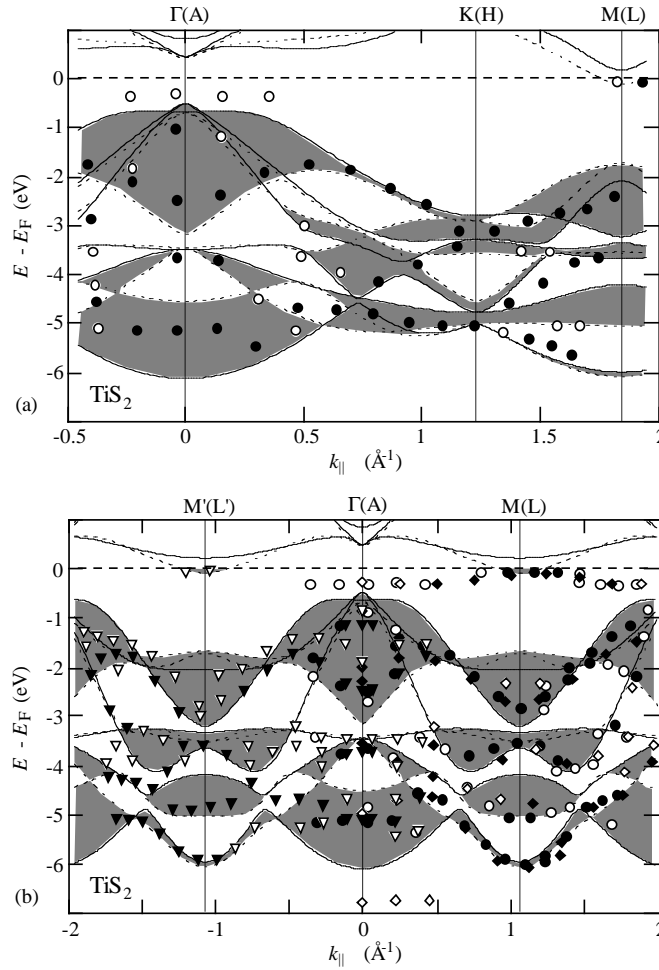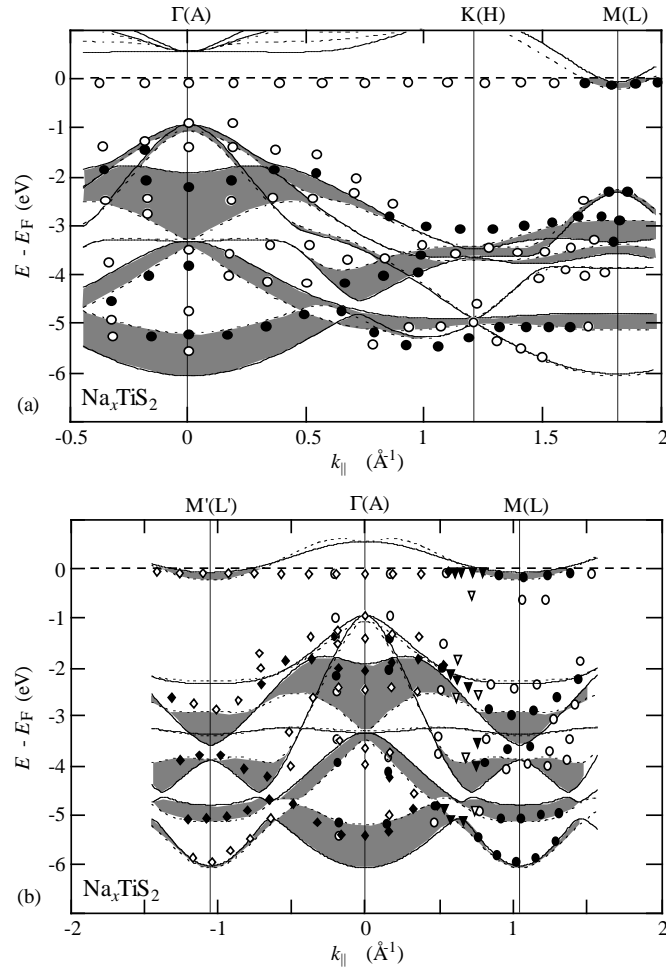

Figure 6. TiS$_2$ structure plots in (a) the $\bar{\Gamma}\bar{K}\bar{M}$ direction and (b) the $\bar{\Gamma}\bar{M}$ direction. Filled symbols correspond to conspicuous spectral peaks and open symbols to weaker structures. The experimental data in (a) were obtained with $h\nu = 24$ eV; in (b) with $h\nu = 24$ eV for the $\bar{\Gamma}\bar{M}$ azimuth (O), $h\nu = 38$ eV for the $\bar{\Gamma}\bar{M}$ azimuth ($\diamond$) and with $h\nu = 24$ eV for the $\bar{\Gamma}\bar{M}'$ azimuth ($\triangledown$). Comparisons are made with the TiS$_2$ LAPW bands calculated along (a) ΓKM (full lines) and AHL (dashed lines) and (b) ΓM (full lines) and AL (dashed lines).

areas between associated bands are therefore also consistent with the calculations. Strictly, the experimental points should be compared to the surface-projected band structure, but the shaded areas are a close approximation to this. Due to n doping by excess Ti, E_F is pinned at the conduction band minimum. The LDA band-gap problem was compensated for by shifting the S 3p bands down by 0.81 eV relative to the Ti 3d bands. Very good overall agreement was found for the valence band after this adjustment, and most spectral features could be identified in terms of calculated bands. A minor discrepancy remains for the valence band maximum: the weak feature in the zone centre just below E_F appears to be of valence band origin, as there is a flat band with similar extent in k-space. This identification puts the valence band maximum ~0.2 eV higher than in the LAPW bands, and the band gap is thereby reduced to 0.20 eV, in agreement with the established value [1–3]. The valence band minimum appears to be at M, while the calculations put it at Γ. This particular deviation is clearly connected with the anomalously weak dispersion found when mapping the lowest band along ΓA in the combined VLEED and ARPES study [55].

The analogous structure plots for $Na_x TiS_2$ and $Cs_x TiS_2$ are compared with the LAPW bands in figures 7 and 8, respectively. The calculated conduction bands were shifted 0.4 eV upwards relative to the valence bands for both $Na_x TiS_2$ and $Cs_x TiS_2$. The agreement between the experimental and calculated bands is remarkable, considering that the structural parameters and stoichiometries are not known. Most of the spectral features can be identified in terms of the calculated bands, but some weak features appearing outside the calculated bands (e.g. 2 eV below E_F near $\bar{K}$ in figure 8(a)) are probably due to indirect transitions or scattering. This applies also to the conduction band emission seen just below E_F: the occupied electron pockets around $\bar{M}$ give rise to strong emission, but a weak structure remains in the rest of the BZ through indirect transitions or scattering, which may result from randomly distributed alkali metal atoms. In principle, ordered alkali metal superlattices could give rise to Umklapp scattering, but no evidence for such contributions was found. Such superlattices have been observed at room temperature in both $Na_x TiS_2$ [57] and $Cs_x TiS_2$ [40] by x-ray and transmission electron diffraction, respectively, but the absence of superlattice spots in LEED suggests that the alkali metal distribution in the near-surface region is disordered. The band-structure characteristics are summarized in table 2. The gap between the Ti 3d and S 3p bands increased from 0.2 to 0.8 and 0.7 eV for $Na_x TiS_2$ and $Cs_x TiS_2$, respectively. The increased p–d gap indicates that the Ti–S bonds became more ionic after intercalation. The total width of the S 3p bands was reduced upon intercalation by 0.8 and 0.5 eV for $Na_x TiS_2$ and $Cs_x TiS_2$, respectively. Probably this reflects the increased S–S separation, both within layers and between them. These changes, as well as the reduced dimensionality upon intercalation, disproves the rigid-band model (RBM), in which it is assumed that the band structure of the intercalation compound is the same as for the host TMDC, with only the filling of the bands being altered. Still, the RBM may be used

Table 2. Experimental band-structure characteristics of pure and alkali-metal-intercalated TiS_2. All entries are binding energies (relative to E_F) in eV. Entries are as in table 1, except that the symmetry points refer to the surface Brillouin zone.

		TiS_2	$Na_x TiS_2$	$Cs_x TiS_2$
Ti 3d	$\bar{M}$	0.1	0.2	0.2
S 3p	$\bar{\Gamma}$	0.3/5.3	1.0/5.5	0.9/5.6
S 3p	$\bar{M}$	2.1/6.1	2.4/6.0	2.4/6.2
S 3p	$\bar{K}$	2.8/5.1	3.1/5.3	3.2/5.1

Figure 7. Na$_x$TiS$_2$ structure plots along (a) the $\bar{\Gamma}\bar{K}\bar{M}$ direction and (b) the $\bar{\Gamma}\bar{M}$ direction. Filled symbols correspond to conspicuous spectral peaks and open symbols to weaker structures. The experimental data in (a) were obtained with $h\nu = 24$ eV; in (b) with $h\nu = 24$ eV for the $\bar{\Gamma}\bar{M}$ azimuth (O) and $\bar{\Gamma}\bar{M}'$ azimuth ($\Diamond$), and with $\psi = 15°$ for $h\nu = 27, 30, 36$ and 42 eV for the $\bar{\Gamma}\bar{M}'$ azimuth ($\triangledown$). Comparisons are made with the NaTiS$_2$ LAPW bands calculated along (a) ΓKM (full lines) and AHL (dashed lines) and (b) ΓM (full lines) and AL (dashed lines).

for a crude, but conceptually simple, description of some important effects of intercalation, i.e. the transfer of alkali metal s electrons to host-layer bands mainly composed of transition metal d states. The general observation that bands calculated for fully intercalated TMDCs are in good agreement with experimental results for samples with much lower alkali metal concentration [17] also suggests that the major band-structure changes take place very early during intercalation, and that the continued intercalation is fairly well described by applying the RBM to the modified band structure.

5.3.2. Conduction band filling. The sizes of the occupied electron pockets around $\bar{M}$ were estimated in a similar manner to that adopted by Barry *et al* [2] and Traum *et al* [58], assuming the pockets to be ellipsoidal. For the TiS$_2$ later intercalated with Cs, the pocket was assumed
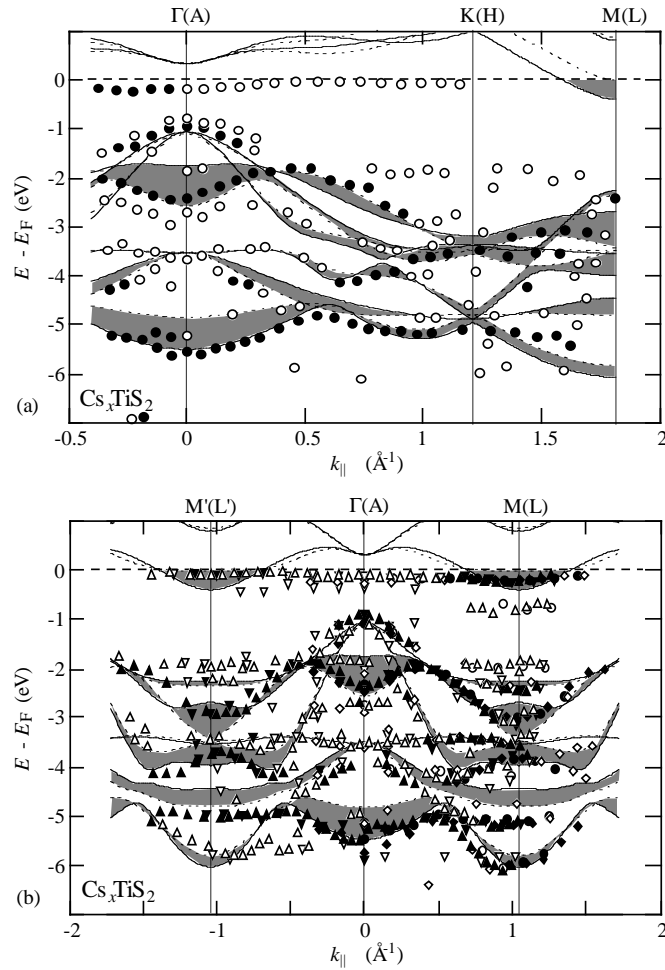
Figure 8. Cs_xTiS_2 structure plots along (a) the $\bar{\Gamma}\bar{K}\bar{M}$ direction and (b) the $\bar{\Gamma}\bar{M}$ direction. Filled symbols correspond to conspicuous spectral peaks and open symbols to weaker structures. The experimental data in (a) was obtained with $h\nu = 21.22$ eV, in (b) with $h\nu = 24$ eV for the $\bar{\Gamma}\bar{M}$ azimuth (O), $h\nu = 21.22$ eV for the $\bar{\Gamma}\bar{M}$ azimuth ($\Diamond$), $h\nu = 21.22$ eV for the $\bar{\Gamma}\bar{M}$ azimuth with $\psi = 15°$ ($\triangledown$) and with $h\nu = 21.22$ eV for the $\bar{\Gamma}\bar{M}'$ azimuth ($\triangle$). Comparisons are made with the $CsTiS_2$ LAPW bands calculated along (a) ΓKM (full lines) and AHL (dashed lines) and (b) ΓM (full lines) and AL (dashed lines).

to extend $\sim$0.25–0.3 Å^{-1} along the ML line in k-space. From the measured EDCs, the lateral extensions along the ΓM and MK lines (semi-major and semi-minor axes) were estimated to be 0.25 and 0.12 Å^{-1} respectively. From this the carrier concentration was calculated to be $(6.5 \pm 1.5) \times 10^{20}$ cm^{-3}, which corresponds to an excess Ti concentration $x \approx 0.01$–0.02. Considering the arbitrariness of the extension along ML and the inaccuracy in determining the Ti 3d Fermi level crossings, the result should be seen as a rough estimate only.

The enlarged electron pockets in Na_xTiS_2 and Cs_xTiS_2 simplified the estimates considerably. The pockets can be modelled as elliptical cylinders along the ML lines. In Na_xTiS_2 the semi-major and semi-minor axes were determined to be 0.41 and 0.24 Å^{-1}, respectively. The corresponding values for Cs_xTiS_2 were 0.4 and 0.2 Å^{-1}. Assuming that

each alkali atom provides one electron to the pocket, the following carrier concentrations and stoichiometries are obtained: $n = (7.0 \pm 1.2) \times 10^{21}$ cm^{-3}, $x = 0.45 \pm 0.1$ for Na$_x$TiS$_2$; and $n = (4.6 \pm 1.2) \times 10^{21}$ cm^{-3}, $x = 0.4 \pm 0.1$ for Cs$_x$TiS$_2$. The occupied bandwidth, taken to be the energy difference between the Ti 3d minimum and E_F, is found to be 0.1 eV for TiS$_2$, 0.19 eV for Na$_x$TiS$_2$ and 0.22 eV for Cs$_x$TiS$_2$. It should be noticed, however, that peaks close to E_F are distorted by the Fermi function, which may shift the spectral peak away from the true band position. In particular, the bandwidth obtained for TiS$_2$ could be excessive for this reason.

5.3.3. Reduced dimensionality. The LAPW calculations predicted reduced perpendicular dispersion of the electronic bands upon alkali metal intercalation, but not the experimentally observed almost complete vanishing of perpendicular dispersion evident from figure 4. One may speculate as to whether this is an effect of larger interlayer separation than assumed, or possibly due to correlation effects restricting the mobility of electrons between the layers, but one should also consider the possibility that the experimental sensitivity to the perpendicular dispersion is somehow lost [17]. Support for this latter explanation is found in figures 7 and 8. The best example of this is perhaps found in figures 8(a) and 8(b), where several structures can be seen near $k_\parallel = 0$ in the energy range 1.5–3 eV BE. It can be argued that they must all be originating from the upper dispersive ΓA band, as there are no other bands in that range. Similar occurrences of multiple features within (or nearly within) the energy range of a single band are found e.g. in the BE ranges 2–3 and 5–6 eV near $k_\parallel = 0$ in figures 7(a) and 7(b), in the BE range 3–4 eV near $k_\parallel = 1$ Å^{-1} in figure 7(b), in the BE range 5–6 eV near $k_\parallel = 0$ in figures 8(a) and 8(b) and in the BE range 3–4 eV near $k_\parallel = -0.7$ Å^{-1} in figure 8(b). As these observations indicate perpendicular dispersions in good agreement with the calculations for both Na$_x$TiS$_2$ and Cs$_x$TiS$_2$, we suggest that the reduction of the dimensionality seems larger than it actually is, due to normal-emission band mapping becoming less sensitive to $k_\perp$.

Reduced ARPES sensitivity to $k_\perp$ is expected when the interlayer spacing is increased, as the BZ then becomes thinner in the layer-perpendicular direction, with more $k_\perp$ averaging as a consequence. The observed effect is too drastic, however, for this to be the only reason. Major loss of $k_\perp$-conservation could result from disorder in the stacking of layers, and there are some results pointing in that direction. Depending on concentration and ionic size, the intercalated alkali can be in either octahedral or trigonal prismatic coordination [20, 21]. For Cs, a 3R stacking with trigonal prismatic coordination is generally expected. At the relatively low concentrations achieved in our experiments, this structure is favoured also for Na. The transformation to the 3R structure requires gliding of adjacent layers, making the conventional unit cell three times larger in the perpendicular direction. However, the rhombohedral primitive unit cell contains the same number of atoms as in the 1T structure, and the surface BZ is unchanged, which is why the band structure should be very similar, especially if the interlayer coupling is weak. Very recently such a 1T $\rightarrow$ 3R transformation was observed by transmission electron microscopy and diffraction for single crystals of TiS$_2$ intercalated *in situ* with Cs, but the transformation was incomplete and accompanied by defect formation [40]. It seems very likely indeed that stacking disorder produced by such incomplete structural transformations is the primary reason for the observed loss of perpendicular dispersion.

6. Conclusions

We have used ARPES to study the electronic structure of pure TiS$_2$ and how it can be modified by *in situ* intercalation with Na and Cs. Both alkali metals intercalated easily, as verified by

core-level spectroscopy.

Remarkably good agreement was found between LAPW bands and experimental band dispersions along the layers. The p–d gap increased significantly upon intercalation, while the total width of the S 3p bands was markedly reduced. The initial electronic structure changes upon intercalation are too extensive to be accurately described in terms of the rigid-band model, but in a modified form it might describe the effects of continued intercalation quite well.

The electronic structure of TiS_2 is of 3D character, in good agreement with calculated LAPW bands. After intercalation, the ARPES data indicated a change towards 2D character. The modification can be explained in terms of charge transfer to the host layers and decoupling of these. The LAPW band calculations predicted reduced band dispersion perpendicular to the layers, although not as much as observed experimentally. A likely explanation for this discrepancy is that the ARPES sensitivity to $k_\perp$ was lost because of stacking disorder induced by an incomplete 1T $\rightarrow$ 3R structural transformation. Further studies of the relation between intercalation and defects are required, as well as a better understanding of $k_\perp$-resolution in ARPES for TMDCs.

Acknowledgments

References

[1] Chen C H, Fabian W, Brown F C, Woo K C, Davies B, DeLong B and Thompson A H 1980 *Phys. Rev.* B **21** 615
[2] Barry J J, Hughes H P, Klipstein P C and Friend R H 1983 *J. Phys. C: Solid State Phys.* **16** 393
[3] Klipstein P C and Friend R H 1984 *J. Phys. C: Solid State Phys.* **17** 2713
[4] Wilson J A and Yoffe A D 1969 *Adv. Phys.* **18** 193
[5] Wilson J A, DiSalvo F J and Mahajan S 1975 *Adv. Phys.* **24** 117
[6] Liang W Y 1986 *Intercalation in Layered Materials* ed M S Dresselhaus (New York: Plenum) p 31
[7] Friend R H and Yoffe A D 1987 *Adv. Phys.* **36** 1
[8] Starnberg H I and Hughes H P 1987 *J. Phys. C: Solid State Phys.* **20** 4429
[9] Weitering H H and Hibma T 1991 *J. Phys.: Condens. Matter* **3** 8535
[10] Pettenkofer C, Jaegermann W, Schellenberger A, Holub-Krappe E, Papageorgopoulos C A, Kamaratos M and Papageorgopoulos A 1992 *Solid State Commun.* **84** 921
[11] Jaegermann W, Pettenkofer C, Schellenberger A, Papageorgopoulos C A, Kamaratos M, Vlachos D and Tomm Y 1994 *Chem. Phys. Lett.* **221** 441
[12] Starnberg H I, Brauer H E, Holleboom L J and Hughes H P 1993 *Phys. Rev. Lett.* **70** 3111
[13] Brauer H E, Starnberg H I, Holleboom L J and Hughes H P 1995 *J. Phys.: Condens. Matter* **7** 7741
[14] Brauer H E, Starnberg H I, Holleboom L J and Hughes H P 1995 *Surf. Sci.* **331–333** 419
[15] Starnberg H I, Brauer H E and Hughes H P 1996 *J. Phys.: Condens. Matter* **8** 1229
[16] Brauer H E, Starnberg H I, Holleboom L J and Hughes H P 1996 *Surf. Sci.* **357+358** 345
[17] Brauer H E, Starnberg H I, Holleboom L J, Strocov V N and Hughes H P 1998 *Phys. Rev.* B **58** 10 031
[18] Koelling D D and Harmon B N 1977 *J. Phys. C: Solid State Phys.* **10** 3107
[19] Ceperley D M and Alder B J 1980 *Phys. Rev. Lett.* **45** 566
[20] Rouxel J 1980 *Physica* B **99** 3
[21] Wiegers G A 1980 *Physica* B **99** 151
[22] Whittingham M S 1978 *Prog. Solid State Chem.* **12** 41
[23] Ashcroft N W and Mermin N D 1976 *Solid State Physics* (New York: Holt, Rinehart and Winston) p 385
[24] Myron H W and Freeman A J 1974 *Phys. Rev.* B **9** 481
[25] Zunger A and Freeman A J 1977 *Phys. Rev.* B **16** 906
[26] Bullett D W 1978 *J. Phys. C: Solid State Phys.* **11** 4501
[27] Isomäki H, von Boehm J and Krusius P 1979 *J. Phys. C: Solid State Phys.* **12** 3239
[28] McCanny J V 1979 *J. Phys. C: Solid State Phys.* **12** 3263
[29] Umrigar C, Ellis D E, Wang Ding-sheng, Krakauer H and Posternak M 1982 *Phys. Rev.* B **26** 4935

[30] Benesh G A, Woolley A M and Umrigar C 1985 *J. Phys. C: Solid State Phys.* **18** 1595
[31] Dijkstra J, van Bruggen C F and Haas C 1989 *J. Phys.: Condens. Matter* **1** 4297
[32] Fang C M, de Groot R A and Haas C 1997 *Phys. Rev.* B **56** 4455
[33] Law A R, Andrews P T and Hughes H P 1991 *J. Phys.: Condens. Matter* **3** 813
[34] Brauer H E 1996 *PhD Thesis* Göteborg University and Chalmers University of Technology
[35] Schärli M, Brunner J, Vaterlaus H P and Lévy F 1983 *J. Phys. C: Solid State Phys.* **16** 1527
[36] Anderson O 1986 *PhD Thesis* Universität Kiel
[37] Ettema A R H F 1993 *PhD Thesis* University of Groningen
[38] Pettenkofer C and Jaegermann W 1994 *Phys. Rev.* B **50** 8816
[39] Starnberg H I, Brauer H E and Strocov V N 1997 *Surf. Sci.* **384** L785
[40] Remškar M, Popović A and Starnberg H I 1999 *Surf. Sci.* B **430** 199
[41] Starnberg H I, Brauer H E and Hughes H P 1997 *Surf. Sci.* **377–379** 828
[42] Fujimori A, Suga S, Negishi H and Inoue M 1988 *Phys. Rev.* B **38** 3676
[43] Faba M G, Gonbeau D and Pfister-Guillouzo G 1995 *J. Electron Spectrosc. Relat. Phenom.* **73** 65
[44] Doniach S and Sunjic M 1970 *J. Phys. C: Solid State Phys.* **3** 285
[45] Wertheim G K and Hüfner S 1975 *Phys. Rev. Lett.* **35** 53
[46] Wertheim G K and Walker L R 1976 *J. Phys. F: Met. Phys.* **6** 2297
[47] Nyholm R, Mårtensson N, Lebugle A and Axelsson U 1981 *J. Phys. F: Met. Phys.* **11** 1727
[48] Wertheim G K, DiSalvo F J and Buchanan N E 1973 *Solid State Commun.* **13** 1225
[49] Shepherd F R and Williams P M 1974 *J. Phys. C: Solid State Phys.* **7** 4416
[50] Straub D and Himpsel F J 1986 *Phys. Rev.* B **33** 2256
[51] Nohara S, Namatame H, Matsubara H, Fujisawa M, Naitou M, Tanaka S, Negishi H, Inoue M, Sakamoto H, Misu A and Suga S 1991 *J. Phys. Soc. Japan* **60** 3882
[52] Strocov V N, Starnberg H I and Ettema A R H F 1995 *Solid State Commun.* **96** 659
[53] Strocov V N, Starnberg H I, Nilsson P O and Holleboom L J 1996 *J. Phys.: Condens. Matter* **8** 7549
[54] Strocov V N, Starnberg H I, Nilsson P O, Brauer H E and Holleboom L J 1997 *Phys. Rev. Lett.* **79** 467
[55] Strocov V N, Starnberg H I, Nilsson P O, Brauer H E and Holleboom L J 1998 *J. Phys.: Condens. Matter* **10** 5749
[56] Hughes H P and Liang W Y 1973 *J. Phys. C: Solid State Phys.* **6** 1684
[57] Hibma T 1980 *J. Solid State Chem.* **34** 97
[58] Traum M M, Margaritondo G, Smith N V, Rowe J E and DiSalvo F J 1978 *Phys. Rev.* B **17** 1836